Electronic Supplementary Material (ESI) for ChemComm.

Boosting CO_2 chemical fixation of MOF-808 by introduction of functional groups and defective Zr sites

Minghui Zhou,[a] Zhengyan Qu,[a] Jiuxuan Zhang,[a] Hong Jiang,[a] Zhenchen Tang*[a,b] and Rizhi Chen*[a,b]

Experimental

Chemicals

Zirconium chloride ($ZrCl_4$), tribenzoic acid (H_3BTC), *p*-aminobenzoic acid, benzoic acid, *p*-iodobenzoic acid, *p*-bromobenzoic acid, *p*-chlorobenzoic acid, *p*-fluorobenzoic acid, and *p*-nitrobenzoic acid, epichlorohydrin (ECH), epoxy butane (EB), allyl glycidyl ether (AGE), styrene oxide (SO), epoxy cyclohexane (ECHE), epoxy cyclopentane (ECP) and epibromohydrin (EBH) were purchased from Shanghai Aladdin Biochemical Technology Co., Ltd., China. Formic acid (FA) was provided by Sinopharm Chemical Reagent Co., Ltd., China. Methanol (MeOH) was obtained from Yonghua Chemical Technology Co., Ltd., China. N, N-dimethylformamide (DMF) was obtained from Shanghai Lingfeng Chemical Reagent Co., Ltd., China. Ethanol was supplied by Yasheng Chemical Co., Ltd., China. The above chemicals were used as received without further purification.

Synthesis of MOF-808 and Y-MOF-808

MOF-808: The preparation of MOF-808 was based on previous work with some modifications. Firstly, 1 mmol tribenzoic acid (H_3BTC) was dissolved in a 40 mL mixture of DMF and formic acid (FA) (V/V, 1/1) with ultrasonic treatment for 10 min. Then 1 mmol zirconium chloride ($ZrCl_4$) was added into the above solution with ultrasonic for 10 min and stirred. After stirring for 1 h at 30 ºC, the solution was transferred to a 100 mL Teflon-lined autoclave and heated at 100 ºC for 24 h. After the reaction was cooled down to room temperature, the white precipitate was recovered by centrifugation and washing with methanol three times and then dried in vacuum at 120 ºC for 12 h.

Y-MOF-808: In a 50 mL beaker, 0.12 g MOF-808 and 1 mmol benzoic acid derivatives containing different substituents (*p*-aminobenzoic acid, benzoic acid, *p*-iodobenzoic acid, *p*-bromobenzoic acid, *p*-chlorobenzoic acid, *p*-fluorobenzoic acid, and *p*-nitrobenzoic acid) were dissolved in DMF (30 mL). The solid–liquid mixture was stirred at 30 ºC for 24 h. After that, the solid was filtered and washed with DMF and ethanol, then dried at 70 ºC overnight.

The final product was named Y-MOF-808 (Y = NH_2, H, I, Br, Cl, F, NO_2, respectively). To investigate the effect of the number of benzoic acid derivatives on the performance of the catalyst, different contents of *p*-fluorobenzoic acid were added under the same synthesis conditions, and the corresponding products were labeled as F-MOF-808-X (X = 0.2, 0.5, 1.5, 2 mmol).

Characterization

Transmission electron microscopy (HRTEM, Talos-F200X) and field emission scanning electron microscopy (FESEM, Hitachi S-4800) were applied for characterizing the microstructures of the catalysts. The specific surface area and pore size distribution of the samples were evaluated by a physical adsorption instrument (Micromeritics ASAP 2020). X-ray diffraction (XRD) patterns were taken on a Rigaku Miniflex 600 diffractometer using Cu Kα radiation (40 kV and 15 mA) at a scan speed of $10^{o}\cdot min^{-1}$. Fourier transform infrared (FT-IR) spectra were obtained on an Agilent Cary660 spectrometer with a scan range of 4000-500 cm^{-1}. The acidic sites of the catalysts were characterized by NH_3 temperature programmed desorption (NH_3-TPD) (BELCAT-A). The thermostability of the samples was investigated by thermogravimetric analysis (TGA) (NETZSCH STA 209F1) under N_2 atmosphere from ambient temperature to 800 ^{o}C with a heating rate of 10 $^{o}C\cdot min^{-1}$. X-ray photoelectron spectroscopy (XPS) analysis was carried out on a Thermo ESCALAB 250 spectrometer with monochromatic Al Kα radiation. ^{1}H nuclear magnetic resonance (^{1}H NMR) and ^{1}C nuclear magnetic resonance (^{1}C NMR) patterns were measured on a JNM-ECZ400S spectrometer. The Zr content was determined by an Optima 2000DV inductively coupled plasma-atomic emission spectroscopy (ICP-AES, Perkin-Elmer).

Evaluation of catalytic capability

Typically, the CO_2 cycloaddition reaction with epoxide was carried out in a 50 mL stainless-steel reactor, and the amount of epichlorohydrin (ECH) and catalysts were controlled with 5 mL and 70 mg, respectively. The catalyst and ECH were placed in the reactor, and the air in the reactor was replaced by CO_2 for three times. Then the reaction was carried out at a specific temperature and pressure. After the reaction, the reactor was cooled to room temperature, and the excessive CO_2 was discharged. The product was quantitatively analyzed by gas chromatography, and the conversion and selectivity were calculated. The catalyst was recovered by filtration method, washed with methanol three times to remove the product adsorbed on the surface of the catalyst, and then dried at 70 ºC for the next run.

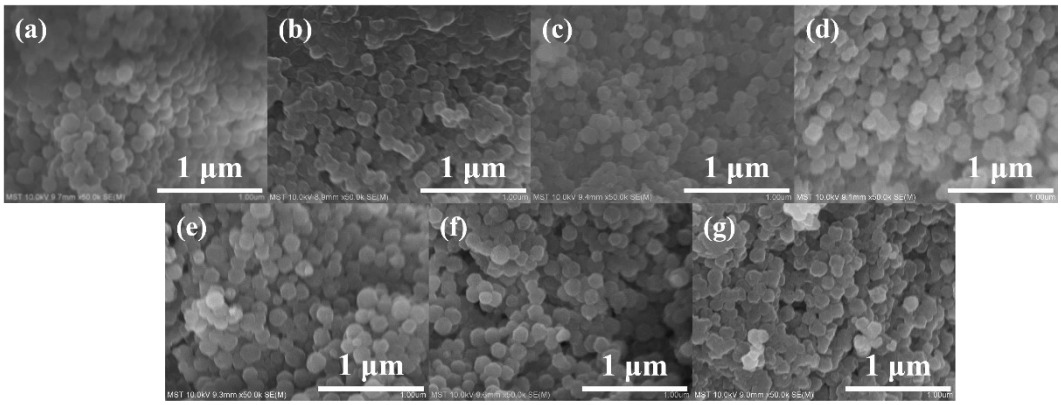

Fig. S1. FESEM images of MOF-808 (a), NH_2-MOF-808 (b), H-MOF-808 (c), I-MOF-808 (d), Br-MOF-808 (e), Cl-MOF-808 (f), NO_2-MOF-808 (g).

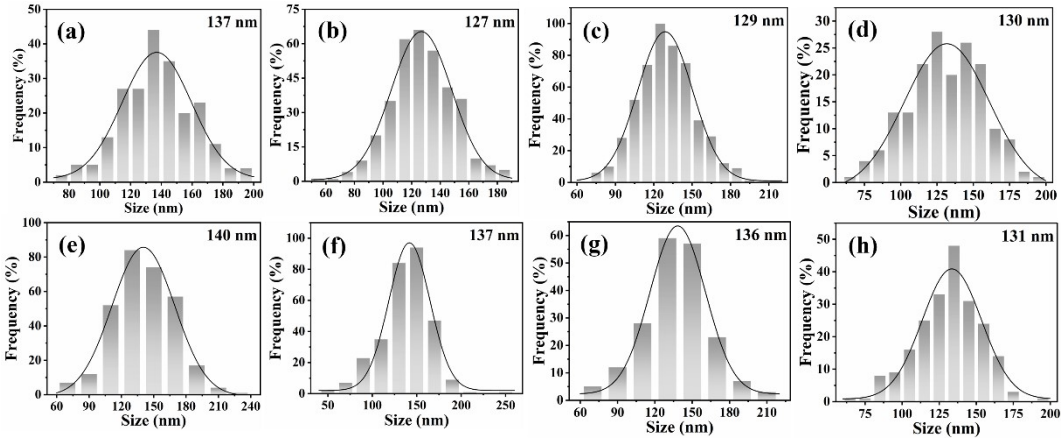

Fig. S2. Particle sizes distribution of MOF-808 (a), NH_2-MOF-808 (b), H-MOF-808 (c), I-MOF-808 (d), Br-MOF-808 (e), Cl-MOF-808 (f), F-MOF-808 (g), NO_2-MOF-808 (h).

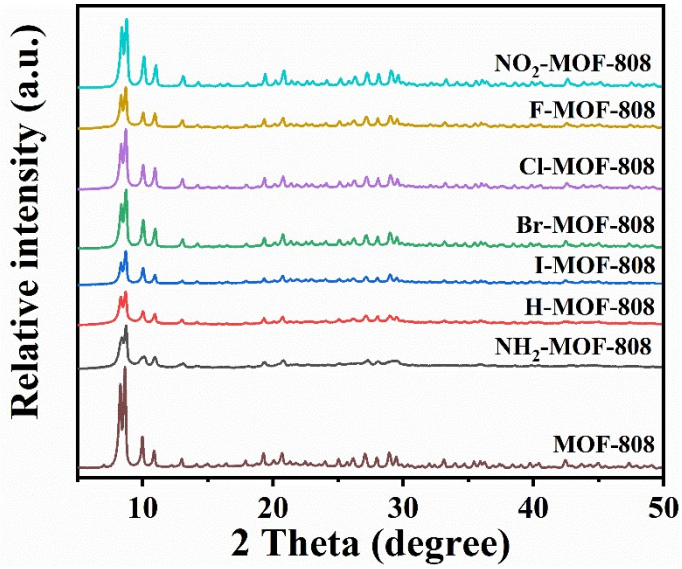

Fig. S3. XRD patterns MOF-808 and Y-MOF-808.

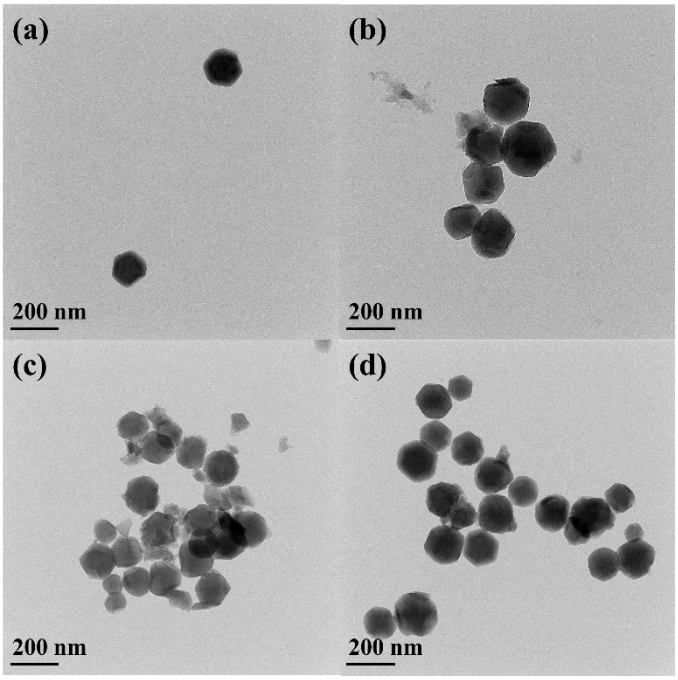

Fig. S4. TEM images of MOF-808 (a), F-MOF-808 (b), NH_2-MOF-808 (c), NO_2-MOF-808 (d)

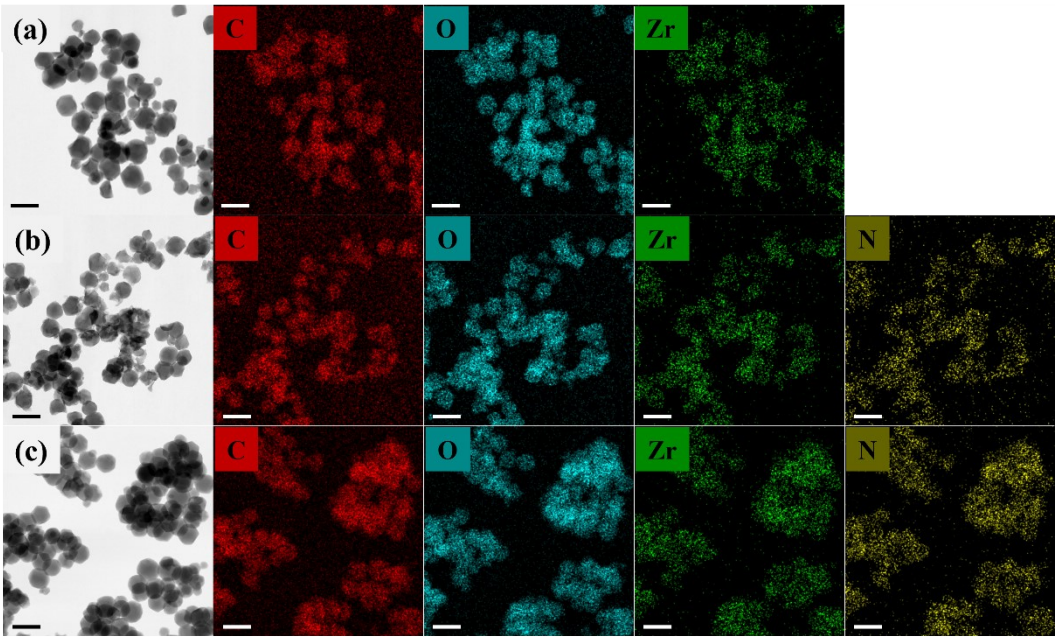

Fig. S5. EDX mapping images of MOF-808 (a), NH_2-MOF-808 (b) and NO_2-MOF-808 (c) (Scale bars: 200 nm).

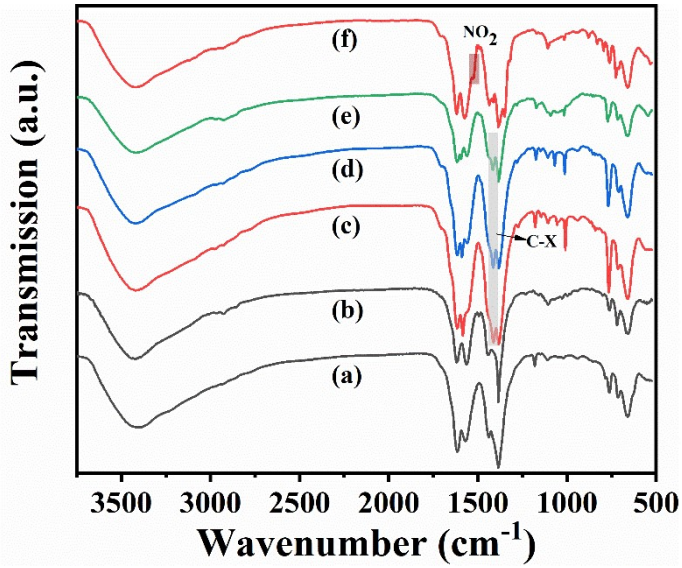

Fig. S6. FT-IR spectra of NH_2-MOF-808 (a), H-MOF-808 (b), I-MOF-808 (c), Br-MOF-808 (d), Cl-MOF-808 (e) and NO_2-MOF-808 (f).

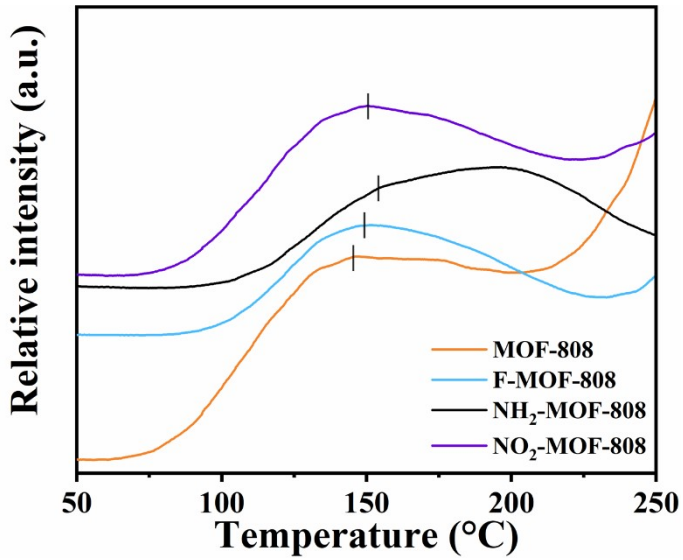

Fig. S7. NH_3-TPD patterns of Y-MOF-808.

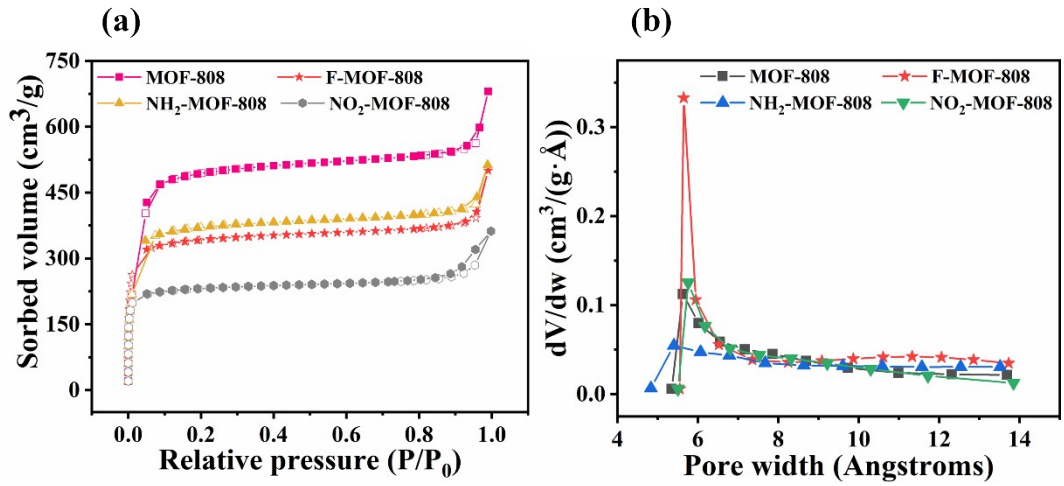

Fig. S8. N_2 adsorption-desorption isothermals (a) and pore diameter distribution curves (b) of theY-MOF-808-

catalysts.

Table S1 Textural properties of the Y-MOF-808 catalysts

Samples	S_{BET} (m^2/g)	V_{pore} (cm^3/g)
MOF-808	1537.6	0.59
F-MOF-808	1158.6	0.44
NH_2-MOF-808	1244.5	0.47
NO_2-MOF-808	788.9	0.31

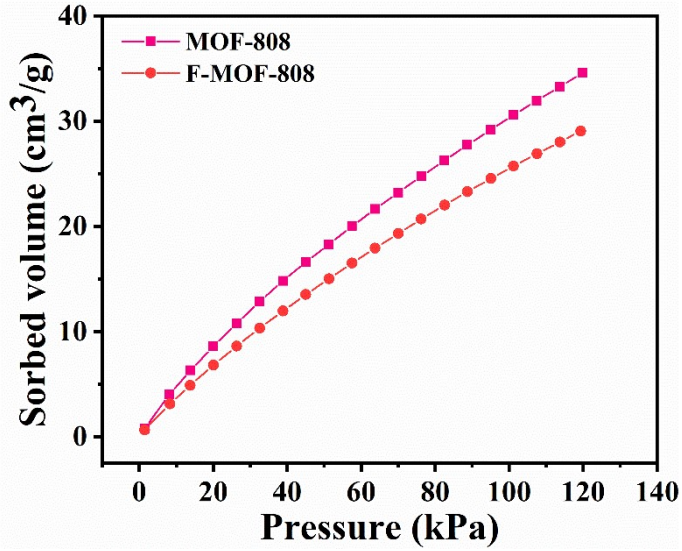

Fig. S9. CO_2 adsorption of MOF-808 and F-MOF-808.

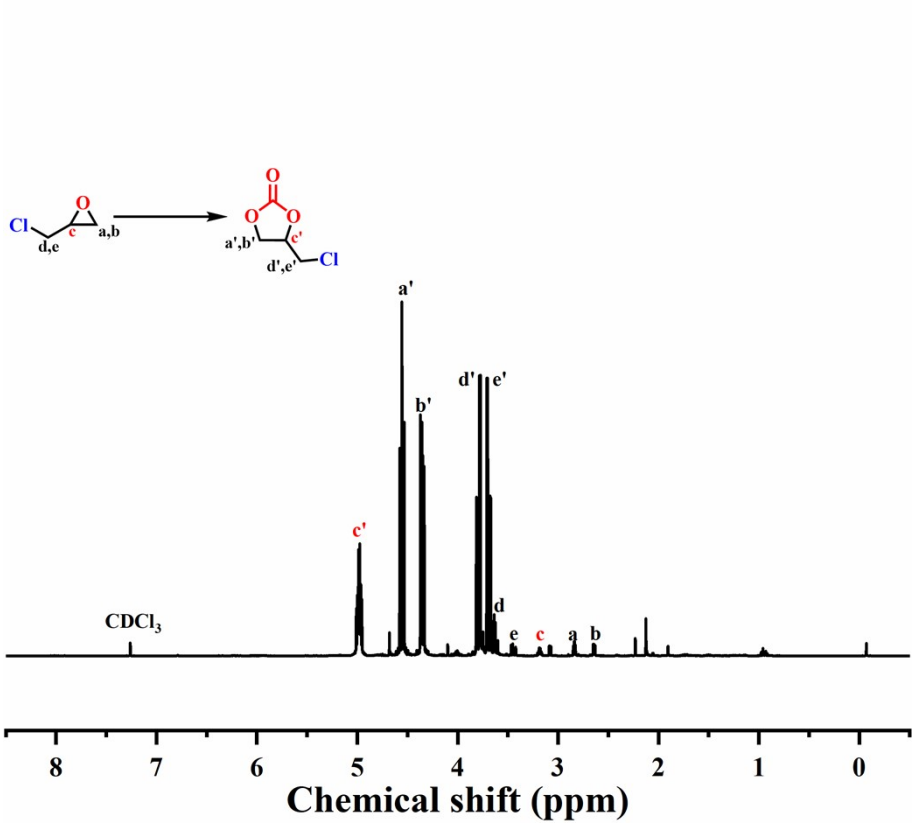

Fig. S10. ^{1}H NMR spectra of epichlorohydrin and its corresponding cyclic carbonate in reaction mixture.

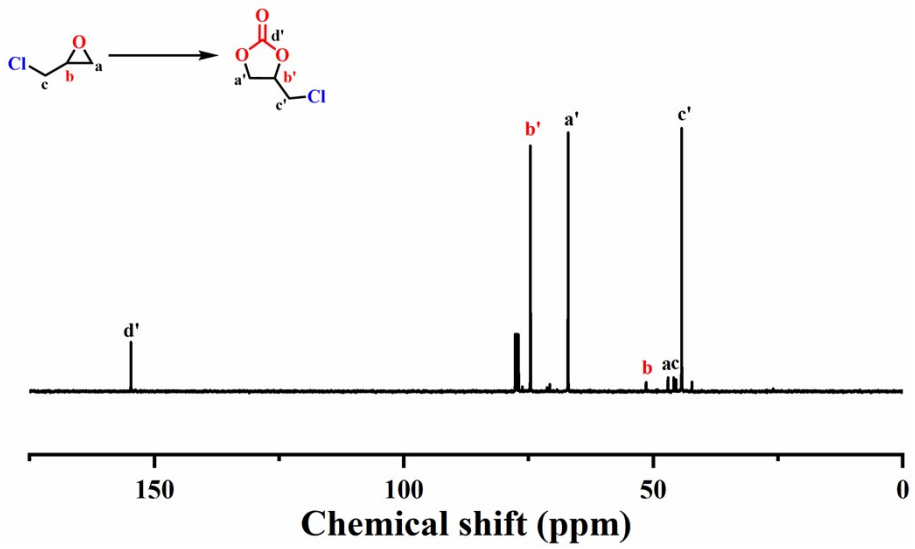

Fig. S11. ^{1}C NMR spectra of epichlorohydrin and its corresponding cyclic carbonate in reaction mixture.

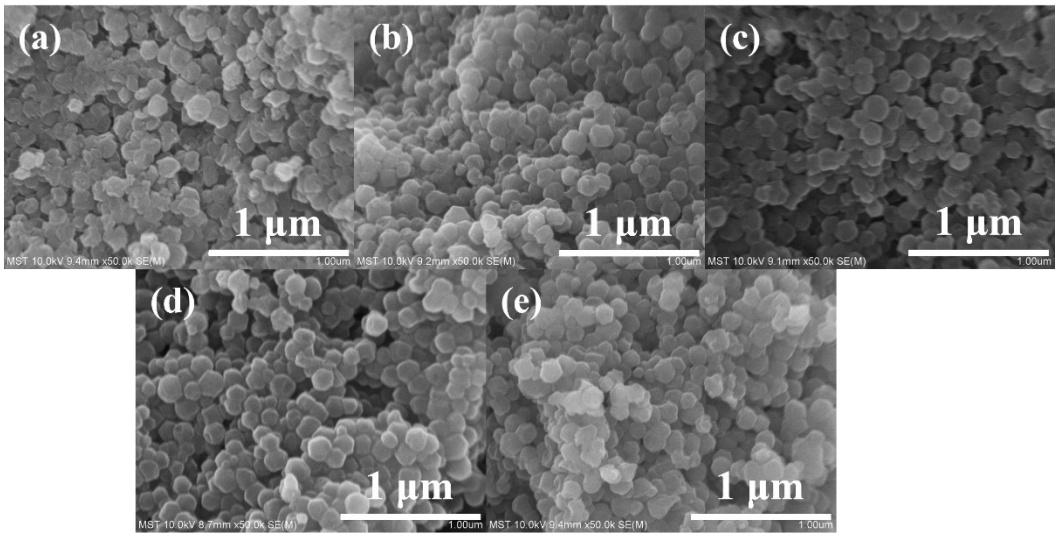

Fig. S12. FESEM images of F-MOF-808-X, X = 0.2 (a), 0.5 (b), 1 (c), 1.5 (d), 2 (e).

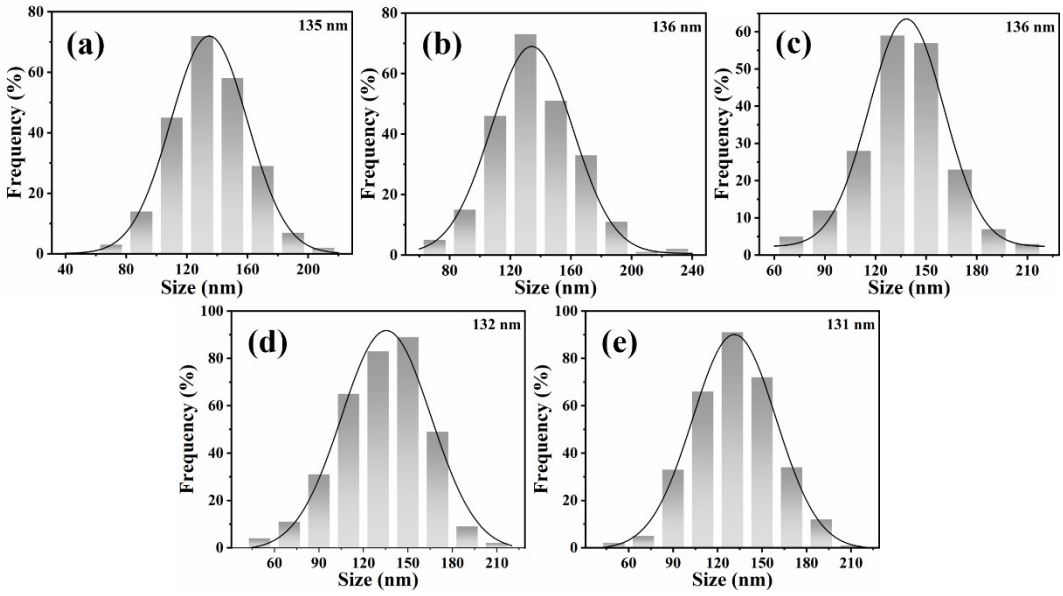

Fig. S13. Particle sizes distribution of F-MOF-808-X, X = 0.2 (a), 0.5 (b), 1 (c), 1.5 (d), 2 (e).

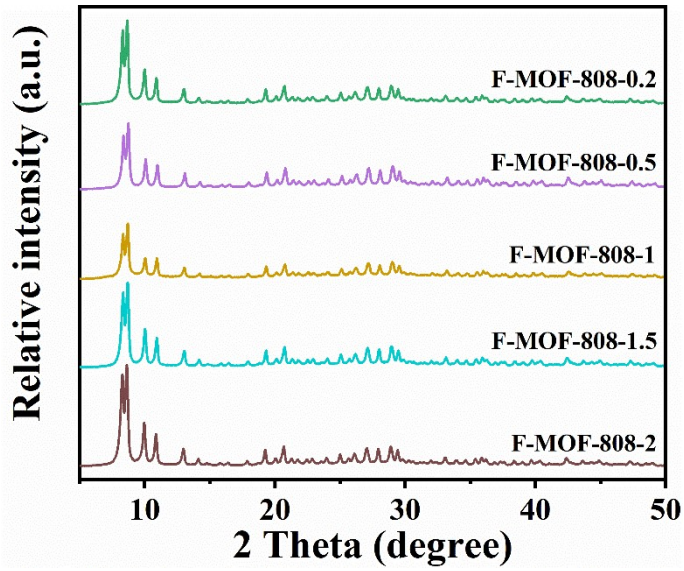

Fig. S14. XRD patterns of F-MOF-808-X.

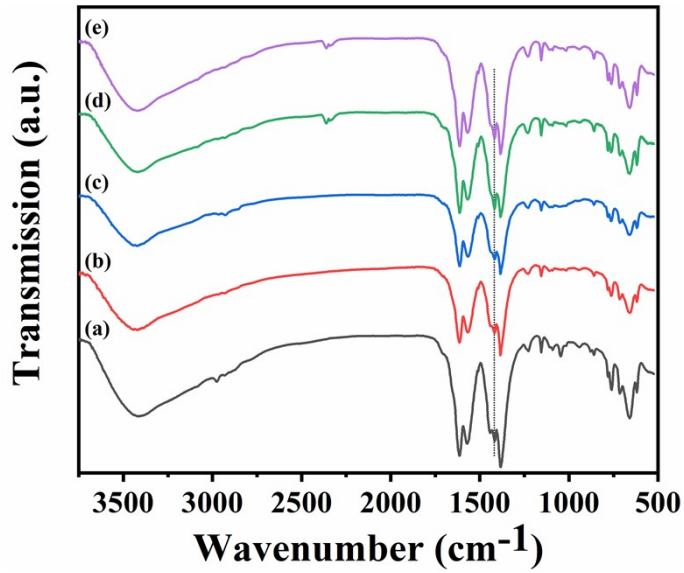

Fig. S15. FT-IR spectra of F-MOF-808-X, X = 0.2 (a), 0.5 (b), 1 (c), 1.5 (d), 2 (e).

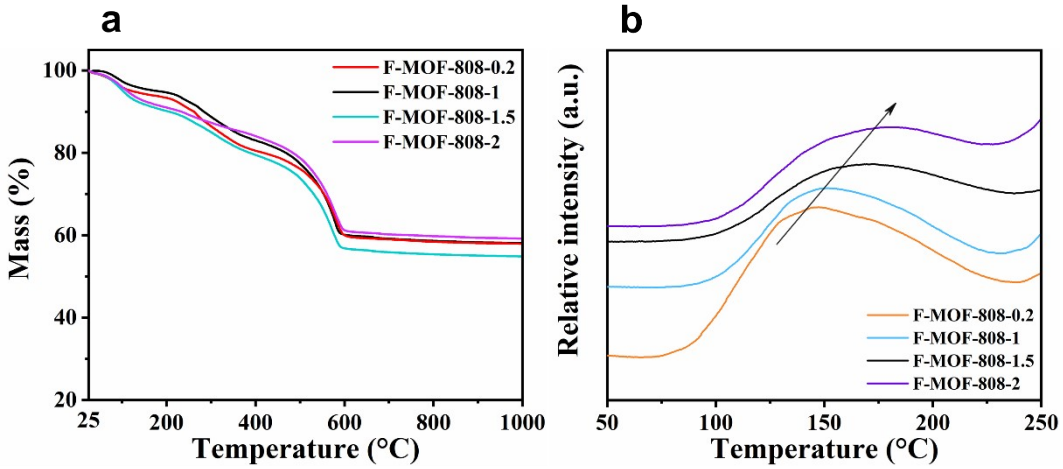

Fig. S16. TG curves (a) and NH_3-TPD patterns (b) of F-MOF-808-X.

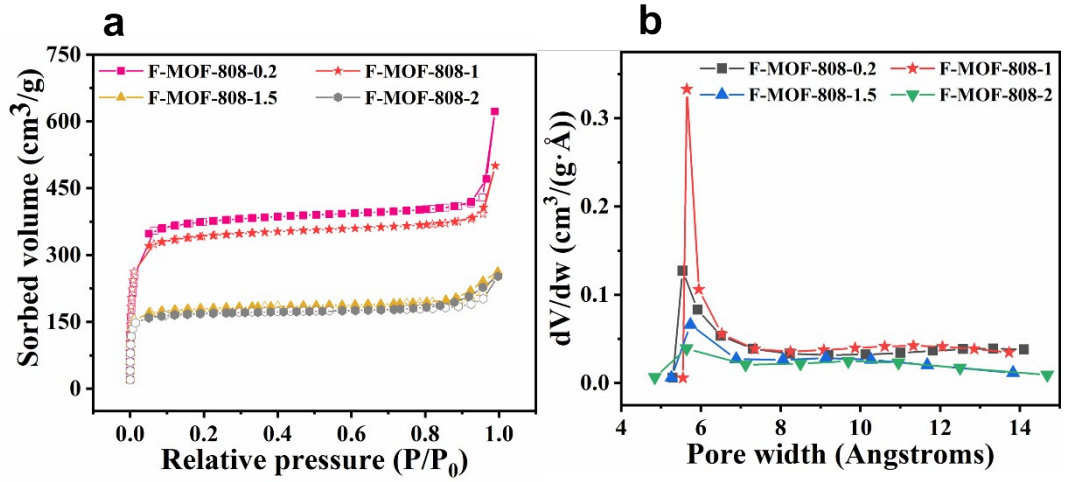

Fig. S17. N_2 adsorption-desorption isothermals (a) and pore diameter distribution curves (b) of the F-MOF-808-X catalysts.

Table S2 Textural properties of the F-MOF-808-X catalysts

Samples	S_{BET} (m^2/g)	V_{pore} (cm^3/g)
F-MOF-808-0.2	1267.5	0.48
F-MOF-808-1	1158.6	0.44
F-MOF-808-1.5	614.1	0.24
F-MOF-808-2	580.9	0.23

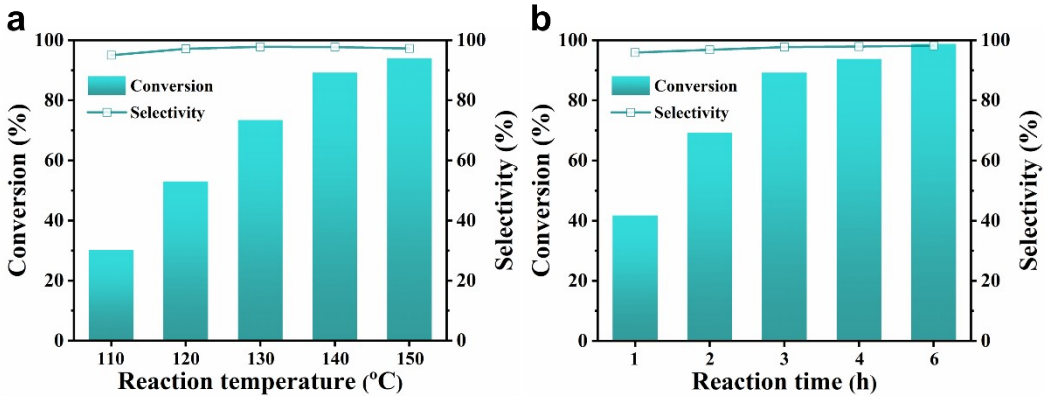

Fig. S18. Catalytic performance of F-MOF-808-1.5 varied with the temperature (a) and time (b) (reaction conditions: ECH = 5 mL, catalyst = 70 mg, P_{CO2} = 0.7 MPa).

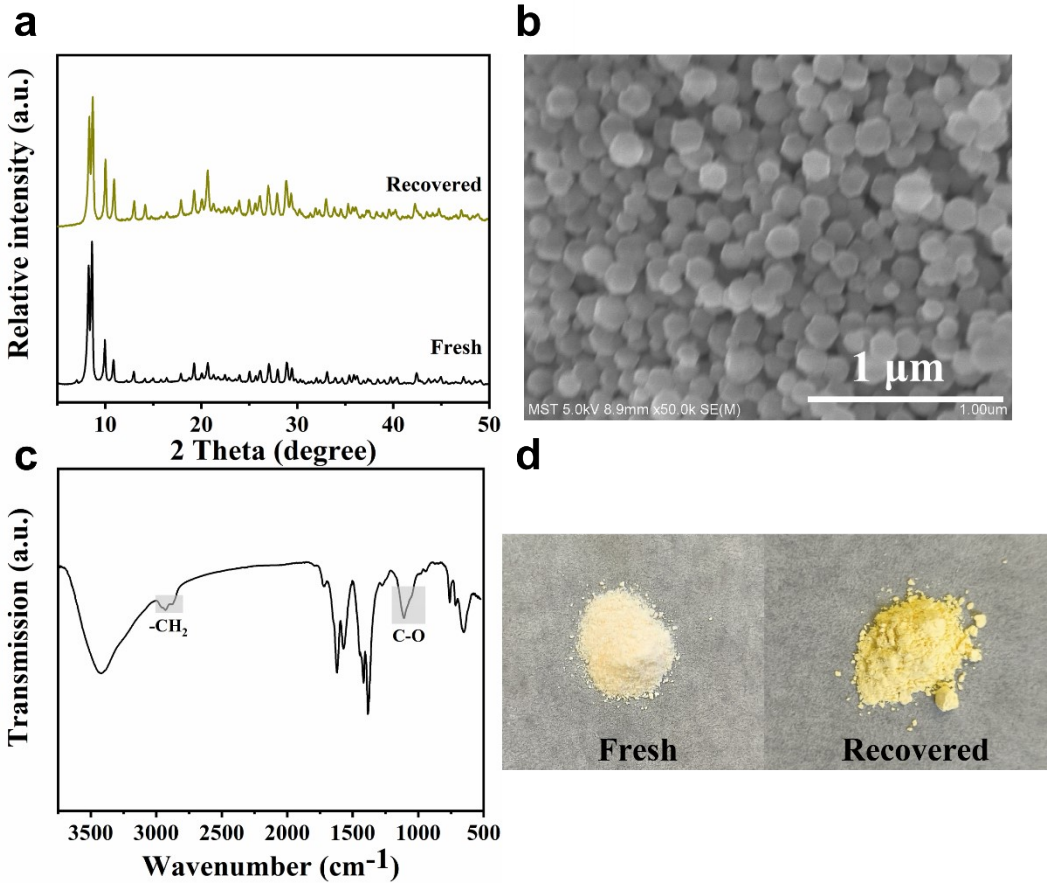

Fig. S19. XRD pattern (a), FESEM image (b), FT-IR spectrum (c) and photographs of the fresh and recovered F-MOF-808-1.5 catalyst after six reaction cycles.

Table S3 The elemental content in the fresh and recovered F-MOF-808-1.5 catalysts

Samples	C 1s (At. %)	O 1s (At. %)	Zr 3d[a] (At. %)	F 1s (At. %)	Zr 3d[b] (Wt. %)
Fresh	35.11	56.24	7.13	1.51	37.82
Recovered	35.45	56.35	6.78	1.42	35.29

[a]Measured by XPS, [b]Measured by ICP-AES

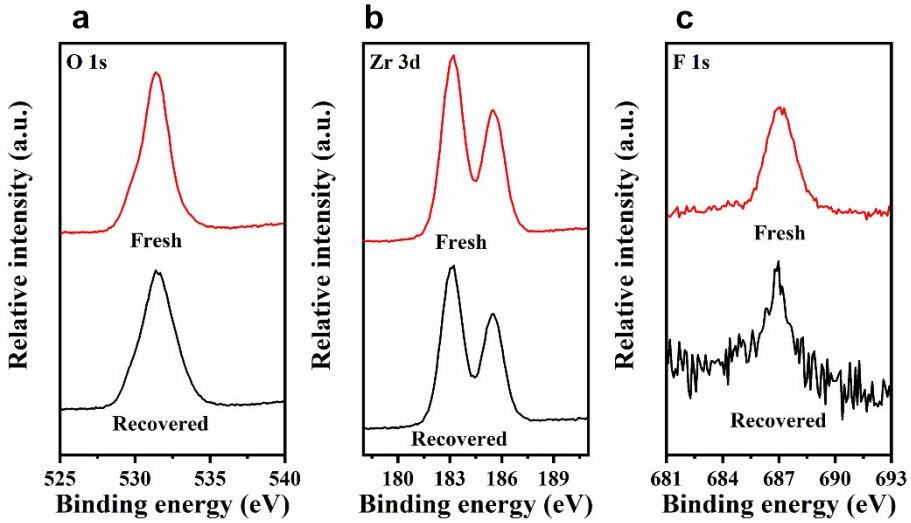

Fig. S20. High-resolution XPS spectra of the fresh and recovered F-MOF-808-1.5: O 1s (a), Zr 3d (b), F 1s (c).

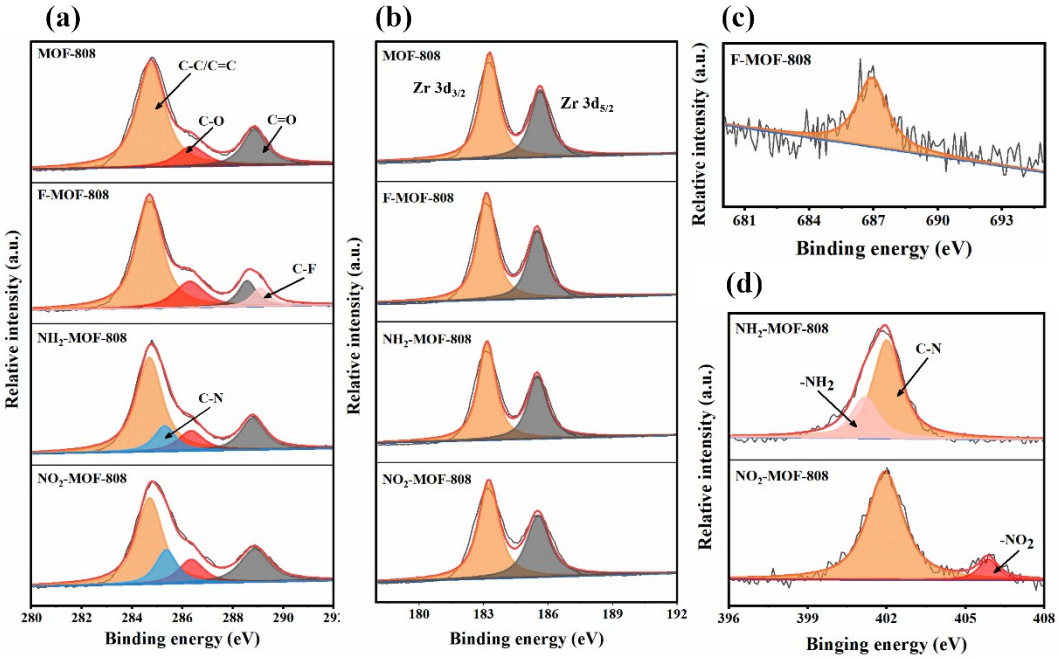

Fig. S21. High-resolution XPS spectra of the Y-MOF-808 catalysts: C 1s (a), Zr 3d (b), F 1s (c), N 1s (d).

Table S4 The surface element content, binding energy of carbon and zirconium of the selected catalysts.

Samples	C 1s (At. %)	O 1s (At. %)	Zr 3d (At. %)	F 1s (At. %)	N 1s (At. %)	C BE (eV)	Zr BE (eV)
MOF-808	35.69	57.48	6.83	/	/	284.77	183.24
F-MOF-808	34.37	57.83	6.87	0.93	/	284.79	183.1
NH_2-MOF-808	35.76	55 .61	6.73	/	1.9	284.78	183.09
NO_2-MOF-808	35.05	56.63	7.02	/	1.3	284.89	183.19

Table S5 Deconvolution results of O 1s peaks of selected catalysts

Samples	Zr-O (At. %)	Zr-O-C (At. %)	C=O (At. %)	N-O (At. %)
MOF-808	23.64	49.62	26.74	/
F-MOF-808	34.03	42.09	22.88	/
NH_2-MOF-808	29.56	45.03	25.41	/
NO_2-MOF-808	26.75	44.75	15.45	13.05

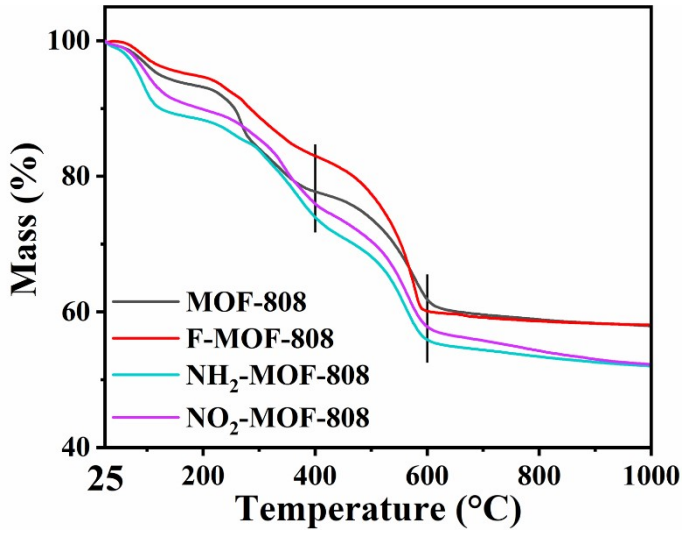

Fig. S22. TG curves of Y-MOF-808.

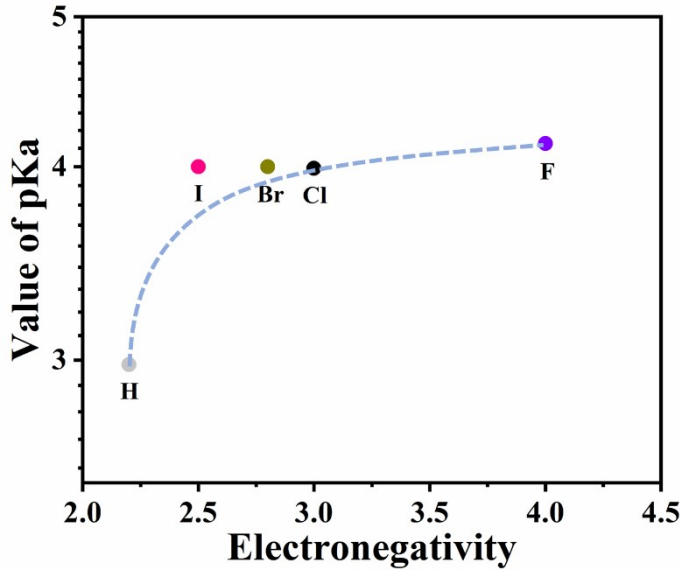

Fig. S23. The correlation of electronegativity with pKa of halogen-substituted benzoic acid.

Table S6 Mass ratio between organic linkers and ZrO_2

Samples	mass ratio (linker /ZrO_2)[a]
MOF-808	0.267
F-MOF-808	0.394
NH_2-MOF-808	0.358
NO_2-MOF-808	0.339

[a]The mass of organic linkers was determined by the weight loss between 400 to 600 °C in TG.

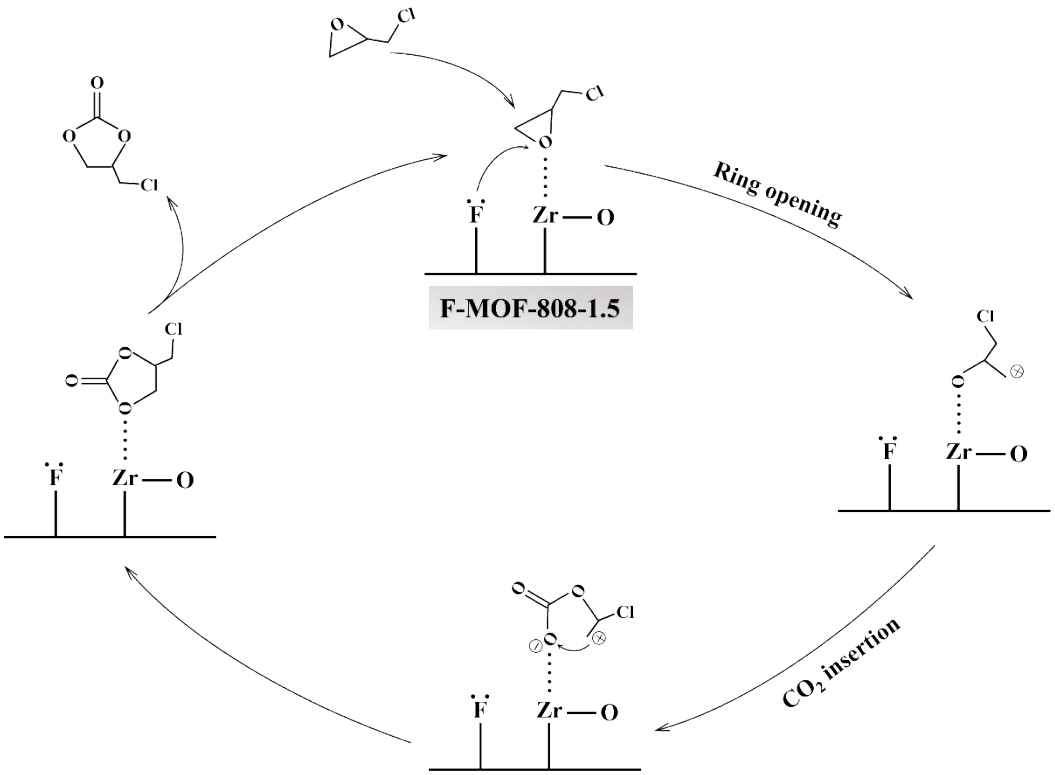

Scheme. S1. Possible reaction mechanism for the CO_2 cycloaddition with ECH over F-MOF-808-1.5.

The possible reaction mechanism of CO_2 cycloaddition with ECH catalyzed by F-MOF-808-1.5 is illustrated in Scheme S1. Initially, ECH is adsorbed on the catalyst surface, where the defect Zr site (Zr-O) and electron-absorbing group (F) initiate ring-opening by attacking the less hindered side of the carbon, leading to the formation of an intermediate containing a carbon cation. Concurrently, CO_2 is activated, generating an oxygen anion and facilitating the subsequent ring-closing reaction to produce cyclic carbonate. Subsequently, the product is desorbed, allowing the catalyst to initiate a new cycle.

Table S7 Comparison of F-MOF-808-1.5 with other MOFs for the cycloaddition of CO_2 with ECH

Samples	Reaction conditions: ECH (mmol), catalyst (mg), temperature (°C), pressure (MPa), time (h)	Con. (%)	Sel. (%)	Reaction rate[a] ($mmol \cdot min^{-1} \cdot g^{-1}$)	Ref.
UiO-66/Cu-BTC	25, 60, 60, 1.2, 8	91	99	0.79	[1]
HImBr@Cr-MIL-101	35.7, 100, 120, 2, 1.5	92.6	100	3.67	[2]
MIL-68(In)-NHTr	10, -, 50, 0.1, 6	28	100	-	[3]
NH_2-MIL-101(Cr)	2, 10, 100, 0.15, 3	99	96	1.1	[4]
UiO-66(30)	20, 50, 80, 1.2, 10	97	100	0.65	[5]
Au/Zn-MOF	10, 36, 70, 3, 6	95 (yield)		0.73	[6]
Zn(dibpca)(OAc)	10, 5, 80, 0.1, 12	89	99	2.47	[7]
ZIF-67	18, 100, 100, 0.8, 8	99	99	0.37	[8]
MIL-101(Cr)-DiT	20, 25, 60, 0.6, 24	100	99	0.56	[9]
USTC-9(Fe)	0.1, 10, 70, 0.1, 24	95.1	99	0.007	[10]
$(Br^-)CH_3$-Pyridinium-MOF-1	20, 100, 90, 0.1, 24	85.6 (yield)		0.12	[11]
CMS@MIL-88-NH_2	10, 50, 80, 0.1, 24	96	100	0.13	[12]
IL@H-Zn/Co-ZIF-50	20, 40, 80, 0.8, 24	99.1	99.3	0.34	[13]
poly ILs@PMo_{12} @CuTCPPCo	12.5, 5, 50, 0.1, 8	98.5 (yield)		5.13	[14]
ZIF-8/CN	4.5, 46, 80, 1, 24	100	100	0.068	[15]
IL@ZIF-8(Zn/Co)	10.8, 100, 100, 0.1, 24	99 (yield)		0.07	[16]
rho-ZMOF (with TBAB)	34.5, 25, 40, 1, 3	98	98.6	7.51	[17]
Co(II)-MOF (with TBAB)	31, 15, 80, 1, 3	97	100	11.14	[18]
F-MOF-808-1.5 with 50 mg TBAB	63.77, 70, 100, 0.7, 4	97.2	98.2	3.7	
MOF-808	63.77, 70, 120, 0.7, 3	26.2	94.2	1.32	This work
F-MOF-808-1.5	63.77, 70, 120, 0.7, 3	53	97.13	2.68	
F-MOF-808-1.5	63.77, 70, 140, 0.7, 3	89.2	97.7	4.52	
F-MOF-808-1.5[b]	63.77, 70, 140, 0.7, 3	75.7	96.2	3.83	

[a] Reaction rate = moles of converted ECH/(reaction time*mass of catalyst)

[b]Catalyst was exposed to humid condition (RH: 70%) for 12 h before the reaction

The catalytic performance of F-MOF-808-1.5 was compared with other previously reported MOF-based heterogeneous catalysts for CO_2 cycloaddition under solvent-free conditions (Table S6). Due to the incorporation of electron-withdrawing groups and a high density of defect sites, F-MOF-808 exhibits superior performance compared to MOF-808 (approximately double that of MOF-808). While the addition of a co-catalyst can enhance catalytic performance, it presents challenges in product purification. In a co-catalyst-free reaction system, our catalyst demonstrates outstanding performance, surpassing most reported MOF-based catalysts. The introduction of ionic liquid into the MOF can enhance catalyst performance,[2, 14] but the associated cost and complex preparation process limit its widespread applications.

References

1. J. Kurisingal, Y. Rachuri, Y. Gu, G. Kim and D. Park, *Appl. Catal. A*., 2019, **571**, 1-11.
2. Q. Li, W. Dai, J. Mao, X. He, Y. Liu, Y. Xu, L. Yang, J. Zou and X. Luo, *Micropor. Mesopor. Mat*., 2023, **350**, 112461.
3. A. Helal, M. Zahir, A. Albadrani and M. Ekhwan, *Catal. Lett*., 2023, **153**, 2883-2891.
4. A. Bezaatpour, M. Amiri, H. Vocke, P. Bottke, M. Zastrau, M. Weers and M. Wark, *J. CO_2 Util*., 2023, **68**, 102366.
5. W. Xiang, J. Ren, S. Chen, C. Shen, Y. Chen, M. Zhang and C. Liu, *Appl. Energ*y, 2020, **277**, 115560.
6. L. Tang, S. Zhang, Q. Wu, X. Wang, H. Wu and Z. Jiang, *J. Mater. Chem. A*., 2018, **8**, 2964.
7. H. Li, X. Zhang, K. Huang and D. Qin, *Polyhedron*, 2022, **220**, 115850.
8. B. Mousavi, S. Chaemchuen, B. Moosavi, Z. Luo, N. Gholampour and F. Verpoort, *New J. Chem*., 2016, **40**, 5170-5176.
9. M. Saghian, S. Dehghanpour and M. Sharbatdaran, *Appl. Organomet. Chem*., 2023, **37**, e6973.
10. W. Han, X. Ma, J. Wang, F. Leng, C. Xie and H. Jiang, *J. Am. Chem. Soc*., 2023, **145**, 9665-9671.
11. J. Xu, S. Peng, Y. Shi, S. Ding, G. Yang, Y. Yang, Y. Xu, C. Jiang and Z. Su, *Daltont*., 2023, **52**, 659-667.
12. C. Duan, Y. Xie, M. Ding, Y. Feng and J. Yao, *J CO_2 Util*., 2022, **64**, 102158.
13. B. Liu, M. Chen, L. Yang, B. Zhao, T. Xia and G. Chang, *Chinese J. Chem. Eng*., 2021, **40**, 124-130.
14. Z. Fang, R. Ren, Y. Wang, Y. Hu, M. Dong, Z. Ye, Q. He and X. Peng, *Appl. Catal. B*., 2022, **318**, 121878.
15. D. Kim, D. Kim, O. Buyukcakir, M. Kim, K. Polychronopoulou and A. Coskun, *Adv. Funct. Mater*., 2017, **27**, 1700706.
16. Y. Sun, X. Jia, H. Huang, X. Guo, and C. Zhong, *J. Mater. Chem. A*., 2020, **8**, 3180.
17. S. Zhang, M. Jang, J. Lee, P. Puthiaraj and W. Ahn, *Acs Sustain. Chem. Eng*., 2020, **8**, 7078-7086.
18. N. Ullah, A. Ramiere, W. Raza, P. Ye, W. Liu, X. Cai, Z. Peng and K. Kim, *J. Colloid. Interf. Sci*., 2022, **623**, 752-761.